

Qubit Energy Tuner Based on Single Flux Quantum Circuits

Xiao Geng,^{1,2,*} Rutian Huang,^{1,2} Yongcheng He,^{1,2} Kaiyong He,^{1,2} Genting Dai,^{1,2} Liangliang Yang,^{1,2}
Xinyu Wu,^{1,2} Qing Yu,^{1,2} Mingjun Cheng,^{1,2} Guodong Chen,^{1,2} Jianshe Liu,^{1,2} and Wei Chen^{1,2,3,†}

¹Laboratory of Superconducting Quantum Information Processing,

School of Integrated Circuits, Tsinghua University, Beijing 100084, China

²Beijing National Research Center for Information Science and Technology, Beijing 100084, China

³Beijing Innovation Center for Future Chips, Tsinghua University, Beijing 100084, China

(Dated: March 7, 2023)

A device called qubit energy tuner (QET) based on single flux quantum (SFQ) circuits is proposed for Z control of superconducting qubits. Created from the improvement of flux digital-to-analog converters (flux DACs), a QET is able to set the energy levels or the frequencies of qubits, especially flux-tunable transmons, and perform gate operations requiring Z control. The circuit structure of QET is elucidated, which consists of an inductor loop and flux bias units for coarse tuning or fine tuning. The key feature of a QET is analyzed to understand how SFQ pulses change the inductor loop current, which provides external flux for qubits. To verify the functionality of the QET, three simulations are carried out. The first one verifies the responses of the inductor loop current to SFQ pulses. The results show that there is about 4.2% relative deviation between analytical solutions of the inductor loop current and the solutions from WRSFQ time-domain simulation. The second and the third simulations with QuTip show how a Z gate and an iSWAP gate can be performed by this QET, respectively, with corresponding fidelities 99.99884% and 99.93906% for only once gate operation to specific initial states. These simulations indicate that the SFQ-based QET could act as an efficient component of SFQ-based quantum-classical interfaces for digital Z control of large-scale superconducting quantum computers.

I. INTRODUCTION

Josephson qubits with gate and measurement fidelities over the threshold of fault-tolerant quantum computing are an attractive candidate for manufacturing scalable quantum computers. As a traditional way for qubit control and readout, microwave electronics succeeded in obtaining gate fidelities beyond 99.9% [1] and realizing quantum supremacy [2]. Because of quantitative restrictions to input and output ports of quantum processor and cryogenic transmission lines, the bottleneck of interconnection comes to be significant when the number of qubits increase beyond a thousand. To overcome the bottleneck, it is desirable to introduce single flux quantum (SFQ) digital logic circuits [3] for control and readout [4]. Digital coherent XY control based on SFQ pulses to transmon qubits was proposed [5] and the fidelities of digital single-qubit gates were measured to be about 95% [6]. Methods of optimization to SFQ pulse sequences for single-qubit gates [7, 8] and two-qubit gates like cross-resonance gates and controlled phase (CZ) gates [9–11] were also studied.

To control qubits flexibly, SFQ-based devices for Z control has become a frontier requiring more research. In 2018, McDermott *et al.* [4] proposed an SFQ-based coprocessor working at 3 K for control and measurement of a quantum processor requiring SFQ-based flux digital-to-analog converters (flux DACs) [12] for Z control, which is really an inspiring idea for creating a scalable superconducting quantum processor. Recently, Mohammad *et*

al. [9] proposed an SFQ-based digital controller called *DigiQ* for superconducting qubits, in which the Z control of qubits are performed with bias currents generated by an array of SFQ/DCs. These SFQ/DCs in *DigiQ* are placed at the 4 K plate of the dilution refrigerator, so bias currents need to be transmitted in superconducting microstrip flex lines to 10 mK plate where the quantum processor works, which is similar to Ref.4.

In order to promote integration further, SFQ logic circuits for control and measurement of qubits should be integrated with quantum processor with 3D integration technologies [13, 14] in the future. Therefore, SFQ-based devices for on-chip Z control need to be researched and designed with circuits as simple as possible for scalable quantum processors. These simple devices should be able to convert SFQ pulse signals to flux signals, just like flux DACs. The circuits for Z control in *DigiQ* may be a little more complicated than flux DACs, so intuitively flux DACs can be considered as the first choice for developing SFQ-based devices for Z control. However, with a single flux DAC defined in Ref.12, it is difficult to provide flux bias and simultaneously complete a Z-control gate with high precision due to the following reasons. (i)The resetting of a flux DAC at the end of the gate can eliminate not only the flux performing the gate but also the bias flux setting the idle frequency of the controlled qubit. (ii)The resetting is accomplished by applying $\Phi_0/2$ (half of a flux quantum) to the two-junction reset SQUID loop, which may require another flux DAC, an SFQ/DC or a pin of the coprocessor for an external current source. This finally increases the physical footprint and complexity of the coprocessor, or aggravates the situation of interconnection bottleneck.

Here, we propose a new SFQ-based device for Z con-

* Email: gengx19@mails.tsinghua.edu.cn

† Email: weichen@mail.tsinghua.edu.cn

trol, which is created from the improvement of flux DACs. Because its basic function is to tune the energy levels of qubits, it is called qubit energy tuner (QET). With flux provided by a QET, the energy levels or the frequency of a flux-tunable transmon qubit can be set to specific levels. At the same time, it can also perform gate operations which need flux bias, such as a Z gate or an iSWAP gate. After a gate operation, the QET can tune the frequency of the qubit back to its idle frequency.

In this article, the circuit structure of QETs is first described in Section II. The key feature of a specific QET is analyzed and an formula is obtained for calculating its inductor loop current providing flux. Next, the ideal Z control method with square-wave-like currents for flux-tunable transmon is described in Section III. Then in Section IV, simulations are done for presenting how the inductor loop current of a QET that provides flux is changed by SFQ pulses and how a QET performs a Z gate and an iSWAP gate. In Section V, the work in this article is concluded. The challenges and opportunities about the QET in the future are discussed.

II. STRUCTURE OF QUBIT ENERGY TUNER

A qubit energy tuner (QET) contains an inductor loop and some flux bias units, positive or negative, as can be seen in FIG. 1. The inductor loop is weakly coupled to the SQUID of a flux-tunable transmon, providing flux for tuning the energy levels of the transmon. A flux bias unit includes a Josephson junction shunted with an inductor, which is coupled to the inductor loop. The Josephson junction can be made of an intrinsic Josephson junction in parallel with a resistor to be an overdamped Josephson junction. The node connected to the Josephson junction and the inductor is treated as an input port of QET for SFQ pulse signal. After receiving an SFQ pulse, a positive flux bias unit increase the external flux through the SQUID by a specific amount while a negative flux bias unit increase it in the opposite direction or decrease it by the same specific amount. This is realized by making the direction of dotted terminals of positive flux bias units the same as that of the corresponding inductor in the inductor loop but making the direction of dotted terminals of negative flux bias units opposite to that of the corresponding inductor in the inductor loop.

A QET should have at least a pair of flux bias units, in which one is positive and the other is negative. In order to tune the energy levels of a transmon more precisely, QET can be designed to have two or more pairs of flux bias units, among which some pairs are used for coarse tuning and others are used for fine tuning. Inductors in different flux bias units can also be coupled for optimization of circuit performance. The inspiration about the qubit energy tuner is from the design of the flux DAC proposed by Ref. 12 and Ref. 15. Therefore, its circuits have similar but simpler structures compared with those of flux DACs.

The QET shown in FIG. 2 is taken as an example for

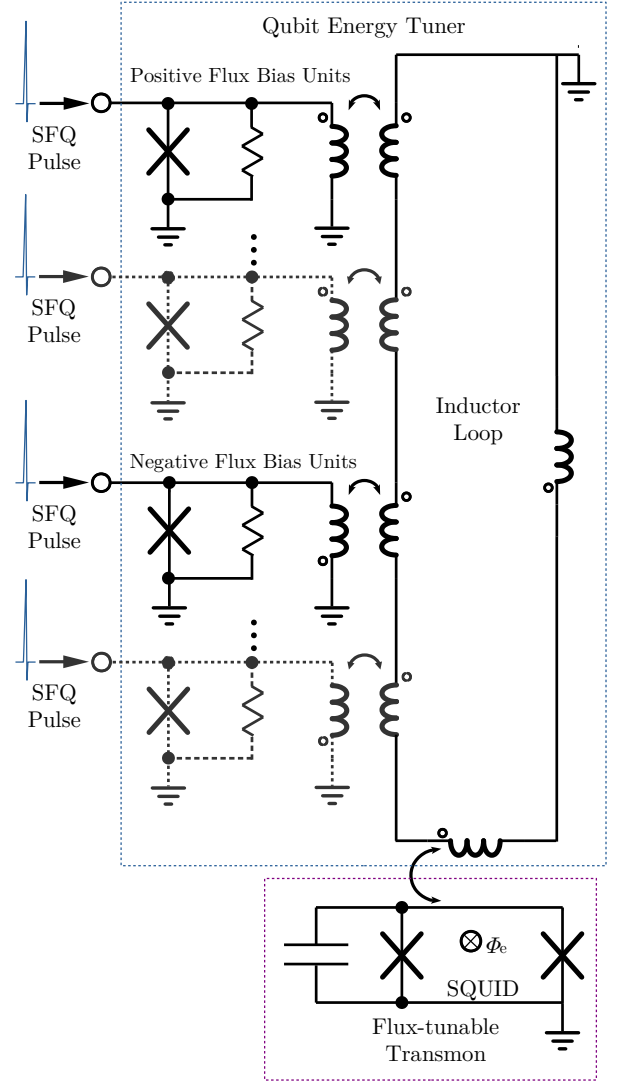


FIG. 1. Structure of a qubit energy tuner coupled with a flux-tunable transmon.

the following analysis. It has a pair of flux bias units for coarse tuning and another pair for fine tuning. The parameters of elements in the example are listed in Table II. The symbol for QET in FIG. 2 is drawn as FIG. 3. The reason why this kind of QET with two pairs of flux bias units is chosen to be analyzed is that it combines the accuracy, simplicity and speed better than other cases with only one or over two pairs of flux bias units. On the one hand, the QET with only a pair of flux bias units has only one precision, which causes a low speed of high-precision tuning or a low precision of high-speed tuning. On the other hand, the QET with three or more pairs of flux bias units have more ports and circuit elements, which means more complicated control, reduced reliability and larger footprint.

According to the formula derivation in Appendix A, by ignoring the influence of SQUID, the current of the

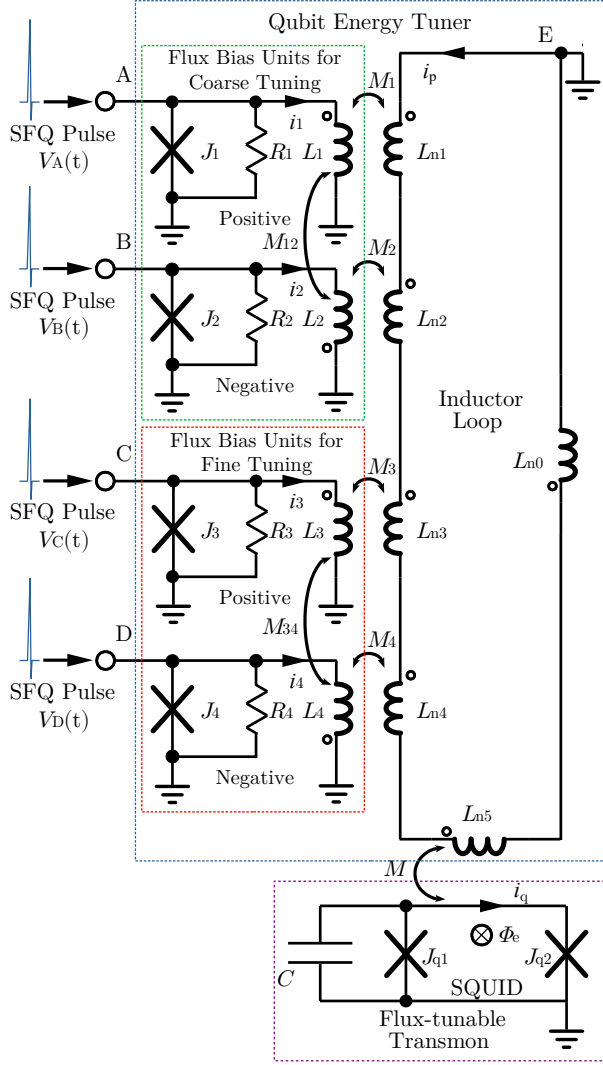


FIG. 2. Schematic of a qubit energy tuner with two pairs of flux bias units for coarse tuning and fine tuning.

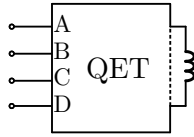


FIG. 3. Symbol of a QET.

inductor loop $i_p(t)$ is approximately equal to

$$i_p(t) = \frac{1}{F} [(\Phi_A - \Phi_B)(L_f^2 - M_{34}^2)(L_c + M_{12})M_c + (\Phi_C - \Phi_D)(L_c^2 - M_{12}^2)(L_f + M_{34})M_f], \quad (1)$$

where Φ_A , Φ_B , Φ_C and Φ_D are the integral of the voltage at node A, B, C and D over time t respectively. Because the input signal to these nodes is SFQ, Φ_A , Φ_B , Φ_C and Φ_D are multiples of flux quantum Φ_0 . F , M_c , M_f , L_c and

L_f are defined in Appendix A.

Then, the relationship between $i_p(t)$ and the external flux through the SQUID Φ_e is

$$\Phi_e = M i_p(t). \quad (2)$$

Denoting

$$\Phi_A - \Phi_B = n_c \Phi_0, \quad (3)$$

$$\Phi_C - \Phi_D = n_f \Phi_0, \quad (4)$$

$$\frac{M}{F} (L_f^2 - M_{34}^2)(L_c + M_{12})M_c = r_c, \quad (5)$$

$$\frac{M}{F} (L_c^2 - M_{12}^2)(L_f + M_{34})M_f = r_f, \quad (6)$$

$$\frac{1}{F} (L_f^2 - M_{34}^2)(L_c + M_{12})M_c \Phi_0 = \Delta i_{pc}, \quad (7)$$

$$\frac{1}{F} (L_c^2 - M_{12}^2)(L_f + M_{34})M_f \Phi_0 = \Delta i_{pf}, \quad (8)$$

$$M \Delta i_{pc} = \Phi_{ec}, \quad (9)$$

$$M \Delta i_{pf} = \Phi_{ef}, \quad (10)$$

yields

$$i_p = n_c \Delta i_{pc} + n_f \Delta i_{pf}, \quad (11)$$

$$\Phi_e = n_c \Phi_{ec} + n_f \Phi_{ef}, \quad (12)$$

$$\Phi_{ec} = r_c \Phi_0, \quad (13)$$

$$\Phi_{ef} = r_f \Phi_0. \quad (14)$$

Equation (12), (13) and (14) mean that the flux provided by QET can be divided into two parts, $n_c \Phi_{ec}$ and $n_f \Phi_{ef}$, which are respectively created by coarse tuning and fine tuning. Φ_{ec} can be regarded as the flux unit of coarse tuning and Φ_{ef} can be regarded as the flux unit of fine tuning. If n_c (or n_f) SFQ pulses are inputted to port A (or C) of the QET, then the external flux through the SQUID will increase by n_c times of Φ_{ec} (or n_f times of Φ_{ef}). Then, if this external flux needs to be eliminated, n_c (or n_f) SFQ pulses should be inputted to port B (or D). Usually for fine tuning r_f is smaller than r_c . If

$$L_c = L_1 = L_{n1} = L_2 = L_{n2}, \quad (15)$$

$$L_f = L_3 = L_{n3} = L_4 = L_{n4}, \quad (16)$$

then the ratio of the flux unit of coarse tuning to the flux unit of fine tuning can be defined as

$$r_{cf} = \frac{\Phi_{ec}}{\Phi_{ef}}. \quad (17)$$

With Equation (3)~(17), there is

$$r_{cf} = \frac{r_c}{r_f} = \frac{\Delta i_{pc}}{\Delta i_{pf}} = \frac{K_c(1 - K_{34})}{K_f(1 - K_{12})}, \quad (18)$$

where the coupling coefficients are

$$K_c = \frac{M_c}{\sqrt{L_1 L_{n1}}} = \frac{M_c}{\sqrt{L_2 L_{n2}}} = \frac{M_c}{L_c}, \quad (19)$$

$$K_f = \frac{M_f}{\sqrt{L_1 L_{n1}}} = \frac{M_f}{\sqrt{L_2 L_{n2}}} = \frac{M_f}{L_f}, \quad (20)$$

$$K_{12} = \frac{M_{12}}{\sqrt{L_1 L_2}} = \frac{M_{12}}{L_c}, \quad (21)$$

$$K_{34} = \frac{M_{34}}{\sqrt{L_3 L_4}} = \frac{M_{34}}{L_f}. \quad (22)$$

The parameter r_{cf} means the ratio of the flux precision of coarse tuning to that of fine tuning. It should have an appropriate value larger than 1, like 10, to distinguish the two precisions. The parameter r_f is the ratio of the smallest variation of the flux Φ_e , Φ_{ef} , to flux quantum Φ_0 , that is, it determines the flux precision of fine tuning. The parameter r_c is the ratio of Φ_{ec} to flux quantum Φ_0 and can be set by $r_c = r_{cf} \cdot r_f$.

To design a QET, the parameters r_{cf} , r_f and r_c are main concerns and should be firstly determined. Then, with constraints including Equation (5), (6), (15), (16), (18)~(22), all parameter values of circuit elements should be tried and iterated to meet the requirements from the higher-level design, for example, the footprint of the QET on the chip is matched with the footprint of the qubit.

III. IDEAL Z CONTROL BY SQUARE-WAVE-LIKE CURRENTS

For a flux-tunable transmon, the ideal case for Z control is that the waveforms of currents producing external flux Φ_e are square-wave-like. In this section how the ideal Z control is performed is discussed.

The Hamiltonian of a flux-tunable transmon [16] is

$$\hat{H} = 4E_C (\hat{n} - n_g)^2 - E_{JS}(\varphi_e) \cos(\hat{\phi}), \quad (23)$$

where

$$E_{JS}(\varphi_e) = E_{J\Sigma} |\cos(\varphi_e)| \sqrt{1 + d^2 \tan^2(\varphi_e)}, \quad (24)$$

is the effective Josephson energy of the SQUID of the transmon with a total Josephson coupling energy of two junctions

$$E_{J\Sigma} = E_{J1} + E_{J2}, \quad (25)$$

a asymmetry coefficient

$$d = \frac{E_{J2} - E_{J1}}{E_{J\Sigma}}, \quad (26)$$

and a reduced external flux

$$\varphi_e = \pi \frac{\Phi_e(t)}{\Phi_0}. \quad (27)$$

E_C is the charging energy of the transmon. n_g is the effective offset charge. \hat{n} and $\hat{\phi}$ are respectively the number operator and the phase operator of Cooper pairs. For convenience, the hats of all operators including Hamiltonian are left out in the following derivation.

The solution for the k^{th} eigen energy of Equation (23) with first order approximation of perturbation theory [16] is

$$E_k = k \sqrt{8E_C E_{JS}(\varphi_e)} - \frac{E_C}{12} (6k^2 + 6k + 3) - E_{JS}(\varphi_e). \quad (28)$$

Usually, the external flux $\Phi_e(t)$ at the moment t for Z control is provided by a conductor line besides the SQUID with its current, $i_z(t)$, and a mutual inductance between the line and the SQUID, M . Because the current in the SQUID is much smaller than $i_z(t)$, its influence on $i_z(t)$ can be ignored and there is

$$\Phi_e(t) = M i_z(t). \quad (29)$$

Therefore, $E_{JS}(\varphi_e)$ can be written as

$$E_{JS}(i_z(t)) = E_{J\Sigma} \left| \cos\left(\pi \frac{M i_z(t)}{\Phi_0}\right) \right| \sqrt{1 + d^2 \tan^2\left(\pi \frac{M i_z(t)}{\Phi_0}\right)}. \quad (30)$$

By changing $i_z(t)$, $E_{JS}(i_z(t))$ can be set to a target value, then the energy level E_k , especially E_0 and E_1 can be tuned so that qubit frequency is set to the corresponding target value. When $E_{JS}(i_z(t))$ is set, the condition $E_{JS}(i_z(t))/E_C \gg 1$ should be guaranteed to make sure that the qubit is transmon. According to Equation (28), we have

$$E_0 = -\frac{E_C}{4} - E_{JS}(\varphi_e), \quad (31)$$

$$E_1 = \sqrt{8E_C E_{JS}(\varphi_e)} - E_C - \frac{E_C}{4} - E_{JS}(\varphi_e), \quad (32)$$

$$E_2 = 2\sqrt{8E_C E_{JS}(\varphi_e)} - 3E_C - \frac{E_C}{4} - E_{JS}(\varphi_e). \quad (33)$$

Therefore, the differences of energy levels are

$$E_{10} = E_1 - E_0 = \sqrt{8E_C E_{JS}(\varphi_e)} - E_C, \quad (34)$$

$$E_{21} = E_2 - E_1 = \sqrt{8E_C E_{JS}(\varphi_e)} - 2E_C, \quad (35)$$

and the anharmonicity of the qubit is

$$\alpha = E_{21} - E_{10} = -E_C. \quad (36)$$

Without losing generality, $i_z(t)$ has a square-wave-like waveform and is set to be

$$i_z(t) = \begin{cases} i_w, & t_s \leq t \leq t_e, \\ i_i, & 0 \leq t < t_s \text{ or } t > t_e, \end{cases} \quad (37)$$

where i_w and i_i are the currents for setting working frequency ω_{qw} and idle frequency ω_{qi} of a transmon, respectively. ω_{qw} is the qubit frequency used for Z control. ω_{qi} is the qubit frequency when it is idle and is determined to be the frequency of the rotating frame [17]. t_s and t_e are the moments when a gate operation starts and ends, respectively. Then, the qubit frequency turns to be

$$\omega_q(t) = \begin{cases} \omega_{qw}, & t_s \leq t \leq t_e, \\ \omega_{qi}, & 0 \leq t < t_s \text{ or } t > t_e, \end{cases} \quad (38)$$

where

$$\omega_{qw} = \left(\sqrt{8E_C E_{JS}(i_w)} - E_C \right) / \hbar, \quad (39)$$

$$\omega_{qi} = \left(\sqrt{8E_C E_{JS}(i_i)} - E_C \right) / \hbar. \quad (40)$$

Here, we denote

$$\Delta\omega_q = \omega_{qw} - \omega_{qi}. \quad (41)$$

With Equation (39), (40) and (41), we have

$$\Delta\omega_q = \sqrt{8E_C} \left(\sqrt{E_{JS}(i_w)} - \sqrt{E_{JS}(i_i)} \right). \quad (42)$$

For an idle qubit, its Hamiltonian is

$$H_0 = \hbar \left(\omega_{qi} a^\dagger a + \frac{\alpha}{2} a^\dagger a^\dagger a a \right). \quad (43)$$

Actually, the time-dependent Hamiltonian of the qubit is

$$H = \hbar \left(\Delta\omega(t) a^\dagger a + \omega_{qi} a^\dagger a + \frac{\alpha}{2} a^\dagger a^\dagger a a \right), \quad (44)$$

where a^\dagger and a are the creation operator and the annihilation operator, respectively, and $\Delta\omega(t)$ is defined by

$$\Delta\omega(t) = \omega_q(t) - \omega_{qi}. \quad (45)$$

$\omega_q(t)$ is the actual frequency of the qubit. We denote

$$H_{dz} = \hbar \Delta\omega(t) a^\dagger a, \quad (46)$$

as the drive Hamiltonian for Z control, so there is

$$H = H_0 + H_{dz}. \quad (47)$$

In the rotating frame, the drive Hamiltonian for Z control turns to be

$$\tilde{H} = H_{dz}, \quad (48)$$

and the corresponding evolution operator in the rotating frame is

$$\tilde{U}_{dz} = \mathcal{T} \exp \left(-i \int_{t_s}^{t_e} \frac{\tilde{H}}{\hbar} dt \right), \quad (49)$$

where \mathcal{T} is chronological operator. With Equation (46), (48) and (49), we have

$$\tilde{U}_{dz} = \mathcal{T} \exp \left(-i a^\dagger a \int_{t_s}^{t_e} \Delta\omega(t) dt \right). \quad (50)$$

In the ideal situation where i_w and i_i are constants, when the qubit is working ($t_s \leq t \leq t_e$), there is $\omega_q(t) = \omega_{qw}$, so $\Delta\omega(t)$ becomes the constant $\Delta\omega_q$:

$$\Delta\omega(t) = \Delta\omega_q = \omega_{qw} - \omega_{qi}, \quad (51)$$

and the Hamiltonian H turns to be

$$H = H_w = \hbar \left(\omega_{qw} a^\dagger a + \frac{\alpha}{2} a^\dagger a^\dagger a a \right). \quad (52)$$

We define

$$\varphi = - \int_{t_s}^{t_e} \Delta\omega(t) dt \quad (53)$$

as the phase shift realized by Z control, and define

$$t_z = t_e - t_s \quad (54)$$

as the gate operation time for Z control. With Equation (42), (51), (53) and (54), we have

$$\begin{aligned} \varphi &= - \Delta\omega_q t_z \\ &= \sqrt{8E_C} \left(\sqrt{E_{JS}(i_i)} - \sqrt{E_{JS}(i_w)} \right) t_z. \end{aligned} \quad (55)$$

And according to Equation (50), the corresponding evolution operator for the qubit turns to be

$$\begin{aligned} \tilde{U}_{dz} &= \begin{pmatrix} 1 & 0 \\ 0 & e^{i\varphi} \end{pmatrix} \\ &= \begin{pmatrix} 1 & 0 \\ 0 & \exp \left(i \sqrt{8E_C} \left(\sqrt{E_{JS}(i_i)} - \sqrt{E_{JS}(i_w)} \right) t_z \right) \end{pmatrix}. \end{aligned} \quad (56)$$

To realize on-chip Z control by SFQ, instead of choosing Z control line, i_i and i_w can be produced by the inductor loop current $i_p(t)$ of a QET, which means making $i_z(t) = i_p(t)$.

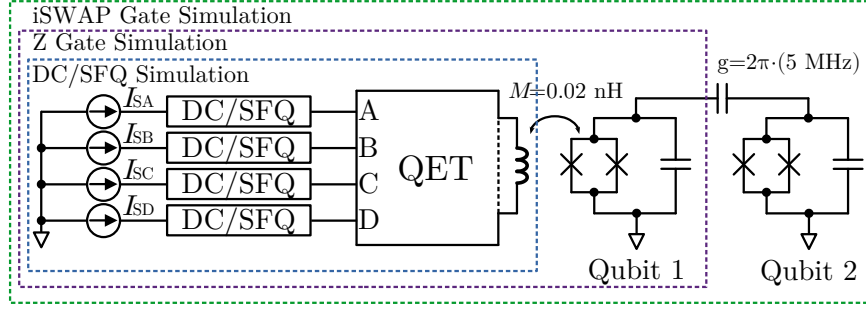


FIG. 4. The circuits for all simulations.

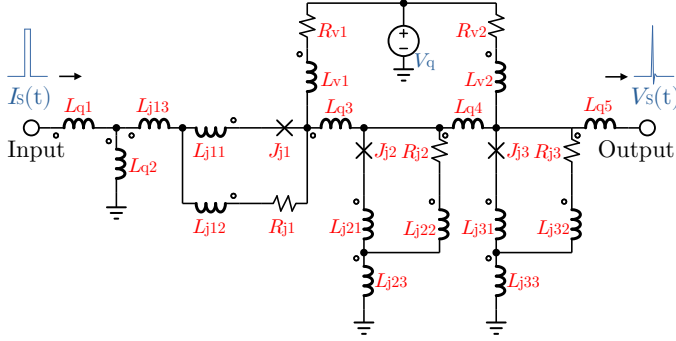


FIG. 5. The simulation circuits of DC/SFQ.

TABLE I. The parameters of elements in the DC/SFQ.

Parameters	Values	Parameters	Values
L_{q1}	1.071 pH	L_{j33}	0.103 pH
L_{q2}	3.927 pH	J_{j1}	225 μ A
L_{q3}	0.913 pH	J_{j2}	225 μ A
L_{q4}	4.399 pH	J_{j3}	250 μ A
L_{q5}	1.090 pH	L_{v1}	16.8 pH
L_{j11}	0.058 pH	L_{v2}	15.5 pH
L_{j12}	0.945 pH	R_{v1}	9.09 Ω
L_{j13}	0.355 pH	R_{v2}	14.29 Ω
L_{j21}	0.05 pH	R_{j1}	0.766 Ω
L_{j22}	0.955 pH	R_{j2}	0.766 Ω
L_{j23}	0.096 pH	R_{j3}	0.688 Ω
L_{j31}	0.028 pH	V_q	2.5 mV
L_{j32}	0.961 pH		

IV. SIMULATION ABOUT A QET AND ITS GATE OPERATIONS

A. a Single QET

In order to show how the inductor loop current $i_p(t)$ of a QET is controlled by SFQ signal, a simulation with superconducting circuit simulation software WRSpipe for

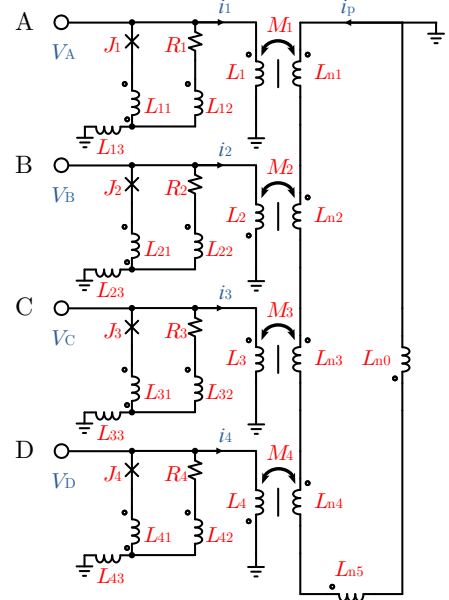


FIG. 6. The simulation circuits of QET.

the circuits in the blue-dashed-line box in FIG. 4 is performed. The SFQ pulses sent to the input ports of QET, A, B, C and D, are generated by four DC/SFQs, each of which is driven by a time-dependent current source. Here, the DC/SFQ is only used for generating SFQ pulses to verify the functionality of the QET. In practical engineering, the QET can also be driven by SFQ pulses from other SFQ digital circuits. The existence and influence of two qubits in FIG. 4 are ignored temporarily. The circuits of DC/SFQ and QET for simulation is shown in FIG. 5 and FIG. 6, and the corresponding parameters of their elements are listed in TABLE I and TABLE II, which are based on the SFQ circuit design data from Ref. 18. In these two tables, the parameters whose names start with letter "J" are the critical currents of corresponding Josephson junctions. The circuit of the QET in FIG. 6 is a little different from FIG. 2 for consideration of the parasitic inductances, but the functions of the QET will not change essentially. FIG. 7 shows the simulation results including the waveforms of (a) the

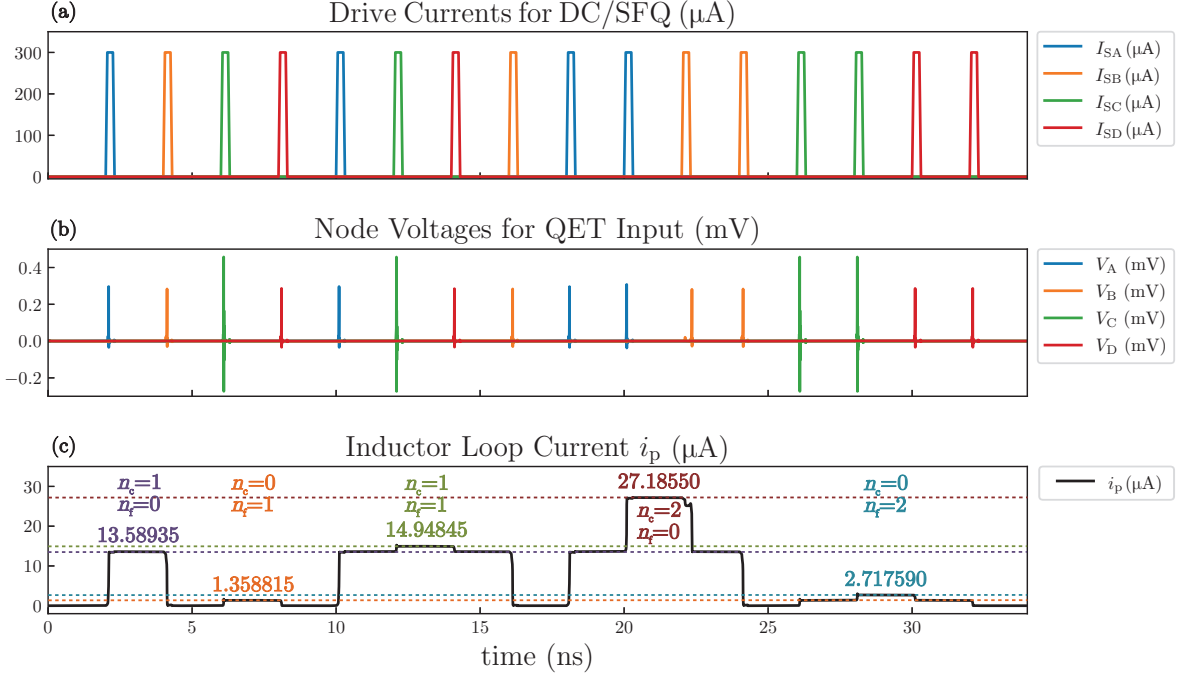


FIG. 7. The responses of QET to SFQ pulses produced by DC/SFQ in simulation.

TABLE II. The parameters of elements in the QET.

Parameters	Values	Parameters	Values
L_1	L_c	L_{11}	0.05 pH
L_2	L_c	L_{12}	0.955 pH
L_3	L_f	L_{13}	0.096 pH
L_4	L_f	L_{21}	0.05 pH
L_c	10 nH	L_{22}	0.955 pH
L_f	10 nH	L_{23}	0.096 pH
L_{n0}	1 nH	L_{31}	0.05 pH
L_{n1}	L_c	L_{32}	0.955 pH
L_{n2}	L_c	L_{33}	0.096 pH
L_{n3}	L_f	L_{41}	0.05 pH
L_{n4}	L_f	L_{42}	0.955 pH
L_{n5}	2 nH	L_{43}	0.096 pH
M_1	M_c	R_1	0.766 Ω
M_2	M_c	R_2	0.766 Ω
M_3	M_f	R_3	0.766 Ω
M_4	M_f	J_1	160 μ A
M_{12}	7.023 nH	J_2	160 μ A
M_{34}	7.023 nH	J_3	160 μ A
M_c	8 nH	J_4	160 μ A
M_f	0.8 nH	M	0.02 nH

drive currents for DC/SFQ, I_{SA} , I_{SB} , I_{SC} and I_{SD} mentioned in FIG. 6; (b) the node voltages for QET input ports, V_A , V_B , V_C and V_D , which are SFQ pulses with time interval 2 ns; (c) the inductor loop current i_p .

TABLE III. The simulation values and analytical values of the inductor loop currents with different n_c and n_f in the simulation for a single QET.

n_c	n_f	Simulation (μ A)	Analytical (μ A)	Relative Deviation (%)
1	0	13.58935	13.03599	4.245
0	1	1.358815	1.303599	4.236
1	1	14.94845	14.33959	4.246
2	0	27.18550	26.07198	4.271
0	2	2.717590	2.607198	4.234

To change the inductor loop current $i_p(t)$ which provides external flux $\Phi_e = Mi_p(t)$, n_c and n_f can be set by the SFQ pulse sequence from DC/SFQ. The simulation and analytical values of the inductor loop current with different n_c and n_f are compared in TABLE III. First, by setting $n_c = 1$ and $n_f = 0$ with SFQ pulses sent to port A and port B (coarse tuning), Δi_{pc} can be extracted from the height of the leftmost lug boss of the inductor loop current curve in FIG. 7(c). The extraction value of Δi_{pc} is 13.58935 μ A, which is close to the value 13.03599 μ A calculated by Equation (7) with relative deviation 4.245%. Similarly, by setting $n_c = 0$ and $n_f = 1$ with SFQ pulses sent to port C and port D (fine tuning), Δi_{pf} can also be extracted as 1.358815 μ A from the second left current lug boss, which is also close to analytical solution 1.303599 μ A from Equation (7) with relative deviation 4.236%. Therefore, the r_{cf} from this simulation is 10.00088 according to Equation (18), almost the same as 10.0, the theory value from analytical solutions.

By setting $n_c = 1$ and $n_f = 1$, the two parts of the inductor loop current correspondingly made by coarse tuning and fine tuning can be accumulated, as shown in the third left lug boss in FIG. 7(c). By setting $n_c = 2$ and $n_f = 0$, the inductor loop current can be double times of Δi_{pc} . Similarly, by setting $n_c = 0$ and $n_f = 2$, the inductor loop current can also be double times of Δi_{pf} . Generally, if the inductor loop current is required to be N_c times of Δi_{pc} plus N_f times of Δi_{pf} , then n_c should be set as N_c and n_f should be set as N_f according to Equation (11).

The waveform of the inductor loop current is similar with composited square waves on the whole, and their rising edges and falling edges are steep, which is helpful for avoiding the crosstalk when the qubit frequency is changing across frequencies of other qubits or resonators, because the qubit frequency is changed quickly enough within time (several picosecond) much shorter than a gate operation time (several nanosecond).

B. Z Gate by a QET

The simulation in this section shows how a QET can perform a Z gate. The circuit for simulation is defined as the circuit in the purple-dashed-line box of FIG. 4, which is based on the circuit of the former simulation in the blue-dashed-line box. The controlled qubit, Qubit 1, is a symmetric flux-tunable transmon connected to the former circuit, so we set $d = 0$ and $E_{J1} = E_{J2} = E_J$. Qubit 2 is ignored temporarily. By controlling the time interval of two SFQ pulses inputted to the port A and B of the QET, the phase of a flux-tunable transmon can be adjusted. Qubit 1 is only driven by coarse tuning with $n_c = 1$, so we set $i_i = 0$ and $i_w = \Delta i_{pc}$, and then $\Delta\omega(t)$ can be approximately treated as the constant $\Delta\omega_q$ when $t_s \leq t \leq t_e$, that is,

$$i_z(t) = i_p(t) = \begin{cases} \Delta i_{pc}, & t_s \leq t \leq t_e, \\ 0, & 0 \leq t < t_s \text{ or } t > t_e, \end{cases} \quad (57)$$

and

$$\Delta\omega_q = \frac{4\sqrt{E_C E_J}}{\hbar} \left(\sqrt{\left| \cos \left(\pi \frac{M \Delta i_{pc}}{\Phi_0} \right) \right|} - 1 \right). \quad (58)$$

Then, with Equation (55) and (58), we have

$$\varphi = \frac{4\sqrt{E_C E_J}}{\hbar} \left(1 - \sqrt{\left| \cos \left(\pi \frac{M \Delta i_{pc}}{\Phi_0} \right) \right|} \right) t_z. \quad (59)$$

The evolution operator \tilde{U}_{dz} turns to be

$$\tilde{U}_{dz} = \begin{pmatrix} 1 & 0 \\ 0 & \exp \left(i \frac{4\sqrt{E_C E_J}}{\hbar} \left(1 - \sqrt{\left| \cos \left(\pi \frac{M \Delta i_{pc}}{\Phi_0} \right) \right|} \right) t_z \right) \end{pmatrix}. \quad (60)$$

By designing the qubit and the QET, the parameters E_C , E_J , M and Δi_{pc} can be determined properly to make t_z in a range easy to realize. Then, for more precise control, the value of t_z should be optimized in practical experiments. Fine tuning can also be performed to compensate gate errors. In this simulation as a simple case, there are $E_J/\hbar = 2\pi \cdot (11.147 \text{ GHz})$, $E_C/\hbar = 2\pi \cdot (148.628 \text{ MHz})$, $M = 0.02 \text{ nH}$, $\Delta i_{pc} = 13.58935 \text{ } \mu\text{A}$. And to realize a Z gate, t_z should be 2.261 ns by solving the equation $\varphi = \pi$. The initial state of Qubit 1 is set to be $|\psi\rangle_{\text{init}} = 1/\sqrt{2}|0\rangle + 1/\sqrt{2}|1\rangle$. The data of $i_p(t)$ is first extracted from its time-domain simulation in WRSpice similar with the former simulation of the single QET without the qubit. Then it is imported to the Z gate simulation program using QuTip [19, 20] to calculate the time-domain data of the drive Hamiltonian for Z control. By calling the function solving master equation or Schrödinger equation of QuTip, like `qutip.mesolve()` or `qutip.sesolve()`, the time-evolution of the qubit state changed by a Z gate operated by the QET can be figured out with a total Hamiltonian H consisting of drive Hamiltonian H_{dz} and idle qubit Hamiltonian H_0 , which is expressed by Equation (47).

The simulation results for a Z gate by the QET in the rotating frame is presented in FIG. 8. Besides the waveforms including (a) drive currents for DC/SFQ, (b) node voltages for QET input and (c) inductor loop current, (d) the frequencies of the qubit eigen energies and (e) the qubit frequency are also plotted in FIG. 8. The black trajectory of the point representing qubit state on the surface of Bloch sphere is drawn in FIG. 9. In this simulation, the gate operation time 2.261 ns is actually controlled by setting the time interval of rising edges of two square-wave pulses in FIG. 8(a). During the period of gate operation (in the lug boss of inductor loop current curve), the qubit frequency is kept at 4.779 GHz with $E_{JS}/E_C = 137.5$, changed from 5.0 GHz with $E_{JS}/E_C = 150$. And the end state of the qubit turns to be $|\psi\rangle_{\text{end}} = 0.70943|0\rangle + (-0.70476 - 0.0049432i)|1\rangle$, which is close to the ideal end state $|\psi\rangle_{\text{iend}} = 1/\sqrt{2}|0\rangle - 1/\sqrt{2}|1\rangle$. The Z gate fidelity for only this time of operation is 99.99884%.

C. iSWAP Gate by a QET

The simulation in this section shows how a QET can perform an iSWAP gate by making the frequency of Qubit 1 the same as that of Qubit 2. Compared with the former simulation for Z gate, the method of this simulation with WRSpice and QuTip remains unchanged, but the simulation circuit is enlarged, as shown in the green-dashed-line box in FIG. 4. The coupling strength between Qubit 1 and Qubit 2 is $g = 2\pi \cdot (5 \text{ MHz})$. The results is presented in FIG. 10. The frequency of Qubit 1 (5.0 GHz) is tuned to the same level as the frequency of Qubit 2 (4.779 GHz) with $i_p = \Delta i_{pc} = 13.58935 \text{ } \mu\text{A}$ by inputting an SFQ pulse to port A of the QET. Then, the QET does nothing for $t_z = 49.16 \text{ ns}$ to wait for state swapping between Qubit 1 and Qubit 2 with the initial

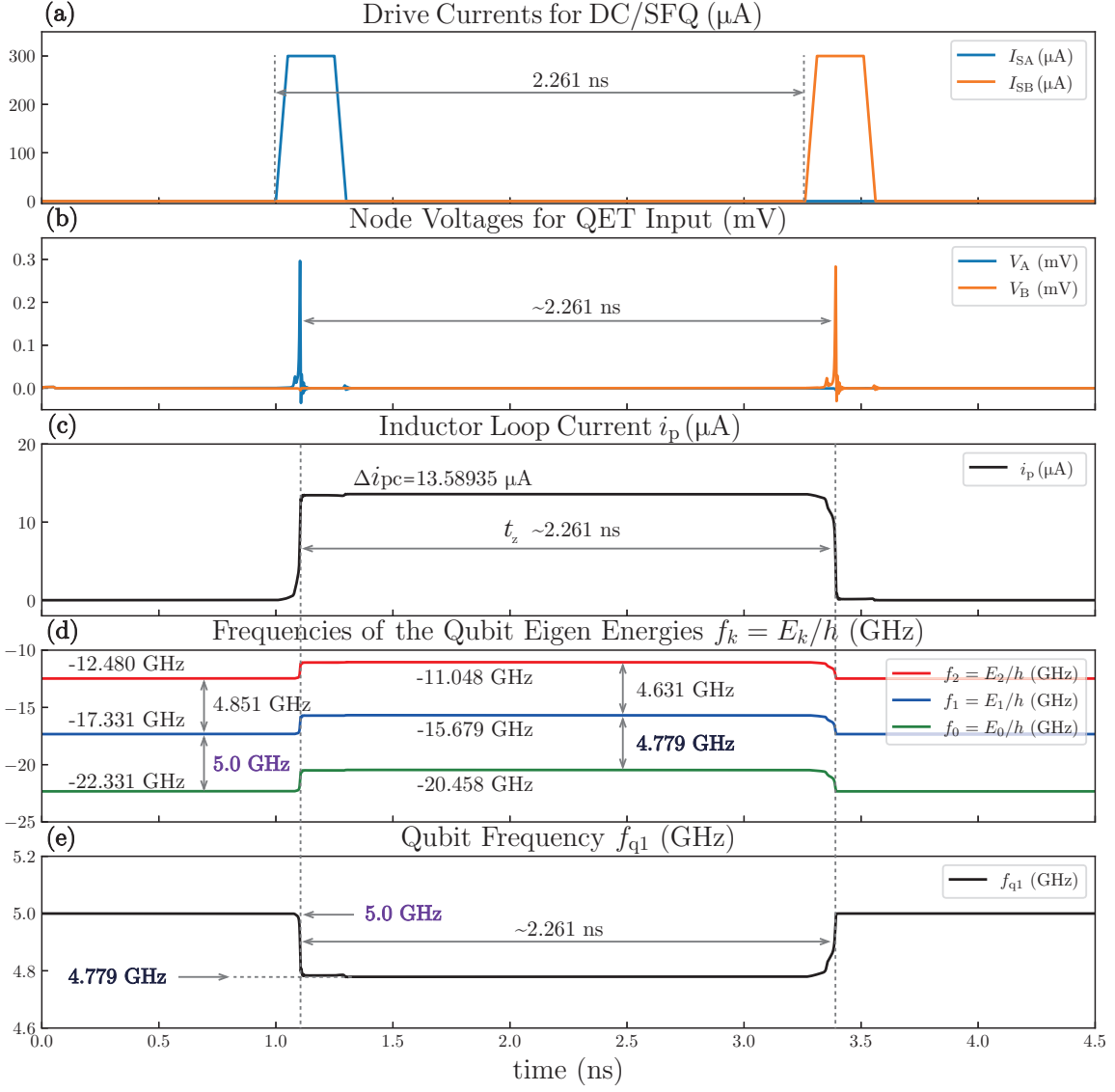


FIG. 8. Z Gate Simulation Results.

state $|\psi\rangle_{\text{init}} = |01\rangle$. When they finished swaping qubit state, the second SFQ pulse is inputted to port B of the QET, which makes Qubit 1 back to its idle frequency. Usually, for two qubits coupling with $g = 2\pi \cdot (5 \text{ MHz})$, the iSWAP gate needs 50 ns. However, here the gate operation time is optimized as 49.16 ns to eliminate the extra phase shift of Qubit 1 caused by changing its frequency and to ensure that the fidelity of the iSWAP gate is high enough at the same time. With the ideal end state $|\psi\rangle_{\text{iend}} = |10\rangle$ and the actual end state $|\psi\rangle_{\text{end}} = (-0.012969 + 0.032406i)|01\rangle + (0.00057846 - 0.99939i)|10\rangle$ in the simulation, the fidelity of the iSWAP gate for only this time of operation is 99.93906%.

V. SUMMARY AND OUTLOOK

In conclusion, we have proposed a device called qubit energy tuner (QET) with description of its circuit structure and theory for its SFQ-based digital Z control to a flux-tunable transmon. A QET can convert SFQ pulses to external flux for qubits, so it is able to set the idle frequency of a flux-tunable transmon and at the same time perform gate operations involving Z control, like Z gates and iSWAP gates, thus paving an approach for digital Z control of an SFQ-based quantum-classical interface, which is highly desirable for the research and development of a large-scale superconducting quantum computer.

For integrating with flux-tunable transmons and avoiding noise from SFQ circuits simultaneously, the parts of QETs consisting of flux bias units can be fabricated on

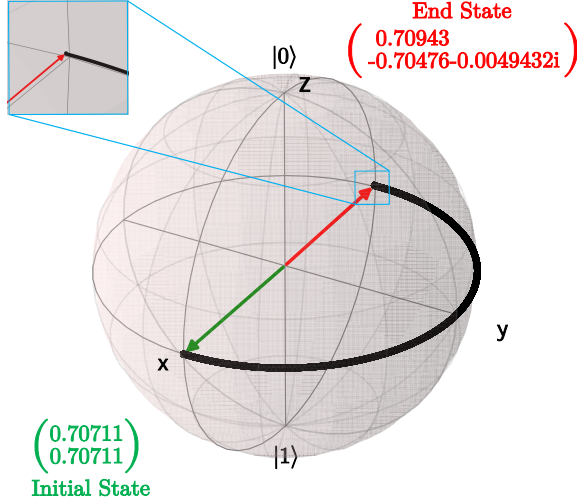


FIG. 9. Trajectory of the point representing qubit state in Z gate simulation (in black).

another substrate which is electrical connected to the qubit chip through silicon vias (TSVs) and indium bumps of a silicon interposer [13, 14]. To realize mutual inductances between transmon SQUIDs and inductor loops of QETs, TSVs and indium bumps should be parts of inductor loops so that the piece of inductor line of an inductor loop for flux bias can be fabricated on the qubit chip or the surface of the silicon interposer faced to qubits. To eliminate the electrical loss of inductor loops, the material of TSVs should be superconductive, e.g. TiN. QETs may also be used in other application scenarios requiring flux tuning, such as CZ gates [21], flux-tunable couplers [22, 23] and qubit readout with a Josephson photomultiplier [24]. As for further research, it is valuable to design and fabricate this device for experiments about SFQ-based digital control of qubits, especially flux-tunable transmons.

ACKNOWLEDGMENTS

This work is partially supported by the key R&D program of Guangdong province (Grant No.2019B010143002).

APPENDIX A. EXTERNAL FLUX OF SQUID FROM THE INDUCTOR LOOP OF QET

According to Kirchhoff's voltage law, the electric potentials of nodes A, B, C, D, E in FIG. 2 are

$$V_A(t') = L_1 \frac{di_1(t')}{dt'} + M_1 \frac{di_p(t')}{dt'} + M_{12} \frac{di_2(t')}{dt'}, \quad (61)$$

$$V_B(t') = L_2 \frac{di_2(t')}{dt'} - M_2 \frac{di_p(t')}{dt'} + M_{12} \frac{di_1(t')}{dt'}, \quad (62)$$

$$V_C(t') = L_3 \frac{di_3(t')}{dt'} + M_3 \frac{di_p(t')}{dt'} + M_{34} \frac{di_4(t')}{dt'}, \quad (63)$$

$$V_D(t') = L_4 \frac{di_4(t')}{dt'} - M_4 \frac{di_p(t')}{dt'} + M_{34} \frac{di_3(t')}{dt'}, \quad (64)$$

$$V_E(t') = L_\Sigma \frac{di_p(t')}{dt'} + M_1 \frac{di_1(t')}{dt'} - M_2 \frac{di_2(t')}{dt'} + M_3 \frac{di_3(t')}{dt'} - M_4 \frac{di_4(t')}{dt'} + M \frac{di_q(t')}{dt'}, \quad (65)$$

where

$$L_\Sigma = L_{n0} + L_{n1} + L_{n2} + L_{n3} + L_{n4} + L_{n5} \quad (66)$$

is the total inductance of the inductor loop obtained by summing self inductances of all parts of the inductor loop. L_1, L_2, L_3 and L_4 are self inductances of inductors in flux bias units. M_1, M_2, M_3 and M_4 are mutual inductances of flux bias units and the inductor loop as shown in FIG. 2. M is the mutual inductance between the inductor loop and the SQUID of flux-tunable transmon. $i_1(t'), i_2(t'), i_3(t'), i_4(t')$ are currents of inductors in flux bias units at the moment t' . $i_p(t')$ and $i_q(t')$ are the current of inductor loop and the SQUID at the moment t' .

Under the zero initial condition, integrating both sides of Equation (61)-(65) with 0 as lower bound and time t as upper bound yields

$$\int_0^t V_A(t') dt' = L_1 i_1(t) + M_1 i_p(t) + M_{12} i_2(t), \quad (67)$$

$$\int_0^t V_B(t') dt' = L_2 i_2(t) - M_2 i_p(t) + M_{12} i_1(t), \quad (68)$$

$$\int_0^t V_C(t') dt' = L_3 i_3(t) + M_3 i_p(t) + M_{34} i_4(t), \quad (69)$$

$$\int_0^t V_D(t') dt' = L_4 i_4(t) - M_4 i_p(t) + M_{34} i_3(t), \quad (70)$$

$$\int_0^t V_E(t') dt' = L_\Sigma i_p(t) + M_1 i_1(t) - M_2 i_2(t) + M_3 i_3(t) - M_4 i_4(t) + M i_q(t). \quad (71)$$

The mutual inductance M is designed to be much smaller than total inductance of the inductor loop L_Σ and other mutual inductances like M_1 for weak coupling to the SQUID of the qubit. And the ring current of the SQUID $i_q(t)$ should be less than the critical current of its Josephson junctions, which is about tens of nA for Al/AlOx/Al

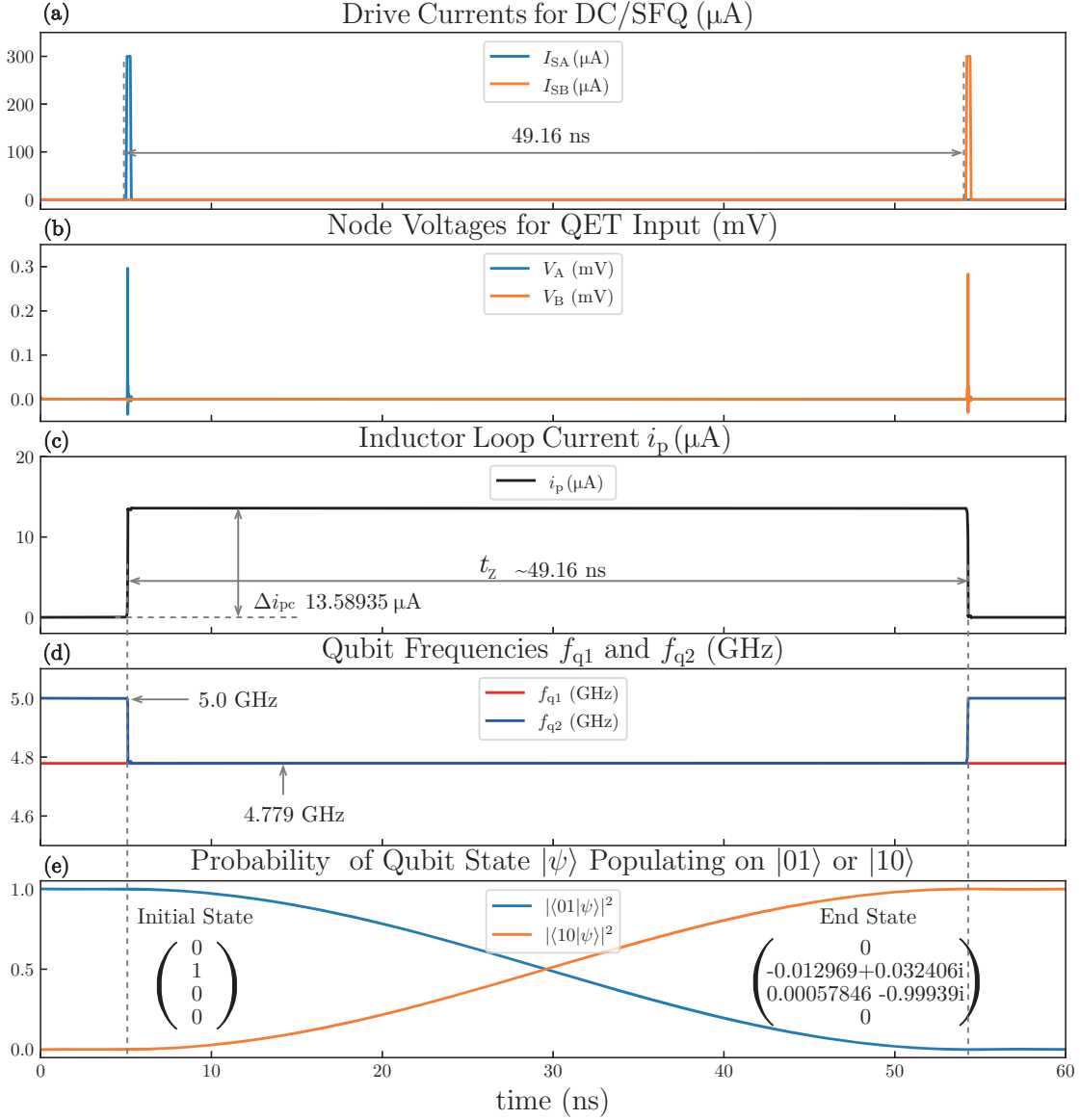


FIG. 10. iSWAP Gate Simulation Result.

junctions and smaller than the current in the inductance loop $i_p(t)$ (about several or tens of mA) by two or more orders of magnitude. Therefore, the influence of the SQUID on the inductance loop, Mi_q , can be ignored in Equation (71), and the electric potential of node E is rewritten as

$$\int_0^t V_E(t')dt' = L_\Sigma i_p(t) + M_1 i_1(t) - M_2 i_2(t) + M_3 i_3(t) - M_4 i_4(t). \quad (72)$$

And then, let

$$\Phi_A(t) = \int_0^t V_A(t')dt', \quad (73)$$

$$\Phi_B(t) = \int_0^t V_B(t')dt', \quad (74)$$

we get

$$\Phi_C(t) = \int_0^t V_C(t')dt', \quad (75)$$

$$\Phi_D(t) = \int_0^t V_D(t')dt', \quad (76)$$

$$\Phi_E(t) = \int_0^t V_E(t')dt', \quad (77)$$

$$\Phi(t) = Li(t), \quad (78)$$

where

$$\Phi(t) = \begin{bmatrix} \Phi_A(t) \\ \Phi_B(t) \\ \Phi_C(t) \\ \Phi_D(t) \\ \Phi_E(t) \end{bmatrix}, \quad (79)$$

$$\mathbf{i}(t) = \begin{bmatrix} i_1(t) \\ i_2(t) \\ i_3(t) \\ i_4(t) \\ i_p(t) \end{bmatrix}, \quad (80)$$

and

$$\mathbf{L} = \begin{bmatrix} L_1 & M_{12} & 0 & 0 & M_1 \\ M_{12} & L_2 & 0 & 0 & -M_2 \\ 0 & 0 & L_3 & M_{34} & M_3 \\ 0 & 0 & M_{34} & L_4 & -M_4 \\ M_1 & -M_2 & M_3 & -M_4 & L_\Sigma \end{bmatrix}. \quad (81)$$

Then, to get $\mathbf{i}(t)$, we have

$$\mathbf{i}(t) = \mathbf{L}^{-1} \Phi(t), \quad (82)$$

where $\mathbf{L}^{-1} = \frac{1}{F} \mathbf{A}$. $\frac{1}{F}$ is the common factor of the elements in the inverse matrix of \mathbf{L} . F is

$$\begin{aligned} F = & L_2(M_{34}^2(L_1L_\Sigma - M_1^2) + 2L_1M_3M_{34}M_4 \\ & + L_3(-L_4(L_1L_\Sigma - M_1^2) + L_1M_4^2) + L_1L_4M_3^2) \\ & + (-L_1M_2^2 - L_\Sigma M_{12}^2 - 2M_1M_{12}M_2)M_{34}^2 \\ & - 2M_{12}^2M_3M_{34}M_4 \\ & + L_3((L_1M_2^2 + L_\Sigma M_{12}^2 + 2M_1M_{12}M_2)L_4 - M_{12}^2M_4^2) \\ & - L_4M_{12}^2M_3^2. \end{aligned} \quad (83)$$

The elements a_{ij} ($i, j = 1, 2, 3, 4, 5$) of \mathbf{A} , are

$$\begin{aligned} a_{11} = & L_2(M_{34}^2L_\Sigma + 2M_3M_4M_{34} \\ & + (-L_4L_\Sigma + M_4^2)L_3 + L_4M_3^2) \\ & + M_2^2(L_3L_4 - M_{34}^2), \\ a_{12} = & M_{12}(-M_{34}^2L_\Sigma - 2M_3M_4M_{34} \\ & + (L_4L_\Sigma - M_4^2)L_3 - L_4M_3^2) \\ & + M_1M_2(L_3L_4 - M_{34}^2), \\ a_{13} = & -(L_4M_3 + M_{34}M_4)(L_2M_1 + M_{12}M_2), \\ a_{14} = & (L_2M_1 + M_{12}M_2)(L_3M_4 + M_3M_{34}), \\ a_{15} = & (L_3L_4 - M_{34}^2)(L_2M_1 + M_{12}M_2), \end{aligned}$$

$$\begin{aligned} a_{21} = & M_{12}(-M_{34}^2L_\Sigma - 2M_3M_4M_{34} \\ & + (L_4L_\Sigma - M_4^2)L_3 - L_4M_3^2) \\ & + M_1M_2(L_3L_4 - M_{34}^2), \\ a_{22} = & L_1(M_{34}^2L_\Sigma + 2M_3M_4M_{34} \\ & + (-L_4L_\Sigma + M_4^2)L_3 + L_4M_3^2) \\ & + M_1^2(L_3L_4 - M_{34}^2), \\ a_{23} = & (L_4M_3 + M_{34}M_4)(L_1M_2 + M_1M_{12}), \\ a_{24} = & -(L_1M_2 + M_1M_{12})(L_3M_4 + M_3M_{34}), \\ a_{25} = & -(L_3L_4 - M_{34}^2)(L_1M_2 + M_1M_{12}), \\ a_{31} = & -(L_4M_3 + M_{34}M_4)(L_2M_1 + M_{12}M_2), \\ a_{32} = & (L_4M_3 + M_{34}M_4)(L_1M_2 + M_1M_{12}), \\ a_{33} = & L_4(L_\Sigma M_{12}^2 + 2M_1M_2M_{12} \\ & + (-L_2L_\Sigma + M_2^2)L_1 + L_2M_1^2) \\ & + M_4^2(L_1L_2 - M_{12}^2), \\ a_{34} = & M_{34}(-L_\Sigma M_{12}^2 - 2M_1M_2M_{12} \\ & + (L_2L_\Sigma - M_2^2)L_1 - L_2M_1^2) \\ & + M_3M_4(L_1L_2 - M_{12}^2), \\ a_{35} = & (L_1L_2 - M_{12}^2)(L_4M_3 + M_{34}M_4), \\ a_{41} = & (L_2M_1 + M_{12}M_2)(L_3M_4 + M_3M_{34}), \\ a_{42} = & -(L_1M_2 + M_1M_{12})(L_3M_4 + M_3M_{34}), \\ a_{43} = & M_{34}(-L_\Sigma M_{12}^2 - 2M_1M_2M_{12} \\ & + (L_2L_\Sigma - M_2^2)L_1 - L_2M_1^2) \\ & + M_3M_4(L_1L_2 - M_{12}^2), \\ a_{44} = & L_3(L_\Sigma M_{12}^2 + 2M_1M_2M_{12} \\ & + (-L_2L_\Sigma + M_2^2)L_1 + L_2M_1^2) \\ & + M_3^2(L_1L_2 - M_{12}^2), \\ a_{45} = & -(L_1L_2 - M_{12}^2)(L_3M_4 + M_3M_{34}), \\ a_{51} = & (L_3L_4 - M_{34}^2)(L_2M_1 + M_{12}M_2), \\ a_{52} = & -(L_3L_4 - M_{34}^2)(L_1M_2 + M_1M_{12}), \\ a_{53} = & (L_1L_2 - M_{12}^2)(L_4M_3 + M_{34}M_4), \\ a_{54} = & -(L_1L_2 - M_{12}^2)(L_3M_4 + M_3M_{34}), \\ a_{55} = & -(L_3L_4 - M_{34}^2)(L_1L_2 - M_{12}^2). \end{aligned}$$

Therefore, we have

$$\begin{aligned} i_p(t) = & \frac{1}{F} (a_{51}\Phi_A(t) + a_{52}\Phi_B(t) \\ & + a_{53}\Phi_C(t) + a_{54}\Phi_D(t) + a_{55}\Phi_E(t)), \end{aligned} \quad (86)$$

that is

$$\begin{aligned} i_p(t) = & \frac{1}{F} (\Phi_A(t)(L_3L_4 - M_{34}^2)(L_2M_1 + M_{12}M_2) \\ & - \Phi_B(t)(L_3L_4 - M_{34}^2)(L_1M_2 + M_1M_{12}) \\ & + \Phi_C(t)(L_1L_2 - M_{12}^2)(L_4M_3 + M_{34}M_4) \\ & - \Phi_D(t)(L_1L_2 - M_{12}^2)(L_3M_4 + M_3M_{34}) \\ & - \Phi_E(t)(L_3L_4 - M_{34}^2)(L_1L_2 - M_{12}^2)). \end{aligned} \quad (87)$$

Because node E is connected to the ground, Φ_E should always be zero. To make the flux bias units of coarse tuning be able to increase or decrease the external flux through the SQUID by the same amount, the following requirements should be met:

$$L_1 = L_2 = L_c, \quad (88a)$$

$$M_1 = M_2 = M_c. \quad (88b)$$

Similarly, for the flux bias units of fine tuning, we have

$$L_3 = L_4 = L_f, \quad (89a)$$

$$M_3 = M_4 = M_f. \quad (89b)$$

Therefore, $i_p(t)$ turns to be

$$i_p(t) = \frac{1}{F}((\Phi_A - \Phi_B)(L_f^2 - M_{34}^2)(L_c M_c + M_{12} M_c) + (\Phi_C - \Phi_D)(L_c^2 - M_{12}^2)(L_f M_f + M_{34} M_f)), \quad (90)$$

and F turns to be

$$F = L_c L_f ((-L_\Sigma L_f + M_f^2) L_c + L_f M_c^2) + (L_f + M_{34})(L_\Sigma L_f - L_\Sigma M_{34} - 2M_f^2) M_{12}^2 + (2L_f^2 M_c^2 - 2M_{34}^2 M_c^2) M_{12} + L_c ((L_\Sigma L_c - 2M_c^2) M_{34}^2 + 2L_c M_f M_f M_{34} + L_c L_f M_f^2 + L_f^2 M_c^2). \quad (91)$$

Hence, the relationship between the current of the inductor loop $i_p(t)$ and the external flux through the SQUID Φ_e is

$$\Phi_e = M i_p(t). \quad (92)$$

-
- [1] R. Barends, J. Kelly, A. Megrant, A. Veitia, D. Sank, E. Jeffrey, T. C. White, J. Mutus, A. G. Fowler, B. Campbell, *et al.*, *Nature* **508**, 500 (2014).
- [2] F. Arute, K. Arya, R. Babbush, D. Bacon, J. C. Bardin, R. Barends, R. Biswas, S. Boixo, F. G. Brandao, D. A. Buell, *et al.*, *Nature* **574**, 505 (2019).
- [3] K. Likharev and V. Semenov, *IEEE Transactions on Applied Superconductivity* **1**, 3 (1991).
- [4] R. McDermott, M. Vavilov, B. Plourde, F. Wilhelm, P. Liebermann, O. Mukhanov, and T. Ohki, *Quantum science and technology* **3**, 024004 (2018).
- [5] R. McDermott and M. Vavilov, *Physical Review Applied* **2**, 014007 (2014).
- [6] E. Leonard Jr, M. A. Beck, J. Nelson, B. G. Christensen, T. Thorbeck, C. Howington, A. Opremcak, I. V. Pechenezhskiy, K. Dodge, N. P. Dupuis, *et al.*, *Physical Review Applied* **11**, 014009 (2019).
- [7] P. J. Liebermann and F. K. Wilhelm, *Physical Review Applied* **6**, 024022 (2016).
- [8] K. Li, R. McDermott, and M. G. Vavilov, *Physical Review Applied* **12**, 014044 (2019).
- [9] M. R. Jokar, R. Rines, G. Pasandi, H. Cong, A. Holmes, Y. Shi, M. Pedram, and F. T. Chong, in *2022 IEEE International Symposium on High-Performance Computer Architecture (HPCA)* (2022) pp. 400–414.
- [10] M. Dalgaard, F. Motzoi, J. J. Sørensen, and J. Sherson, *npj Quantum Information* **6**, 1 (2020).
- [11] M. R. Jokar, R. Rines, and F. T. Chong, in *2021 IEEE International Conference on Quantum Computing and Engineering (QCE)* (2021) pp. 402–412.
- [12] M. Johnson, P. Bunyk, F. Maibaum, E. Tolkacheva, A. Berkley, E. Chapple, R. Harris, J. Johansson, T. Lanting, I. Perminov, *et al.*, *Superconductor Science and Technology* **23**, 065004 (2010).
- [13] D. Rosenberg, D. Kim, R. Das, D. Yost, S. Gustavsson, D. Hover, P. Krantz, A. Melville, L. Racz, G. Samach, *et al.*, *npj quantum information* **3**, 1 (2017).
- [14] D. Rosenberg, S. J. Weber, D. Conway, D.-R. W. Yost, J. Mallek, G. Calusine, R. Das, D. Kim, M. E. Schwartz, W. Woods, *et al.*, *IEEE Microwave Magazine* **21**, 72 (2020).
- [15] P. I. Bunyk, E. M. Hoskinson, M. W. Johnson, E. Tolkacheva, F. Altomare, A. J. Berkley, R. Harris, J. P. Hilton, T. Lanting, A. J. Przybysz, *et al.*, *IEEE Transactions on Applied Superconductivity* **24**, 1 (2014).
- [16] J. Koch, M. Y. Terri, J. Gambetta, A. A. Houck, D. I. Schuster, J. Majer, A. Blais, M. H. Devoret, S. M. Girvin, and R. J. Schoelkopf, *Physical Review A* **76**, 042319 (2007).
- [17] P. Krantz, M. Kjaergaard, F. Yan, T. P. Orlando, S. Gustavsson, and W. D. Oliver, *Applied Physics Reviews* **6**, 021318 (2019).
- [18] G. Li, *Research on Superconducting RSFQ Circuit for Qubit Control*, Ph.D. thesis, Tsinghua University (2018).
- [19] J. Johansson, P. Nation, and F. Nori, *Computer Physics Communications* **183**, 1760 (2012).
- [20] J. Johansson, P. Nation, and F. Nori, *Computer Physics Communications* **184**, 1234 (2013).
- [21] Y. Xu, J. Chu, J. Yuan, J. Qiu, Y. Zhou, L. Zhang, X. Tan, Y. Yu, S. Liu, J. Li, *et al.*, *Physical Review Letters* **125**, 240503 (2020).
- [22] Y. Chen, C. Neill, P. Roushan, N. Leung, M. Fang, R. Barends, J. Kelly, B. Campbell, Z. Chen, B. Chiaro, *et al.*, *Physical review letters* **113**, 220502 (2014).
- [23] F. Yan, P. Krantz, Y. Sung, M. Kjaergaard, D. L. Campbell, T. P. Orlando, S. Gustavsson, and W. D. Oliver, *Physical Review Applied* **10**, 054062 (2018).
- [24] A. Opremcak, I. Pechenezhskiy, C. Howington, B. Christensen, M. Beck, E. Leonard Jr, J. Suttle, C. Wilen, K. Nesterov, G. Ribeill, *et al.*, *Science* **361**, 1239 (2018).